GSI

GSI-Preprint-97-14
Februar 1997

INVARIANT-MASS SPECTROSCOPY OF ^{10}LI AND ^{11}LI

M. Zinser, F. Humbert, T. Nilsson, W. Schwab, H. Simon, T. Aumann, M.J.G. Borge, L.V. Chulkov, J. Cub, Th.W. Elze, H. Emling, H. Geissel, D. Guillemaud-Mueller, P.G. Hansen, R. Holzmann, H. Irnich, B. Jonson, J.V. Kratz, R. Kulessa, Y. Leifels, H. Lenske, A. Magel, A.C. Mueller, G. Münzenberg, F. Nickel, G. Nyman, A. Richter, K. Riisager, C. Scheidenberger, G. Schrieder, K. Stelzer, J. Stroth, A. Surowiec, O. Tengblad, E. Wajda, E. Zude

(Submitted to Nuclear Physics A)

Gesellschaft für Schwerionenforschung mbH
Planckstraße 1 • D-64291 Darmstadt • Germany
Postfach 110552 • D-64220 Darmstadt • Germany

Invariant-Mass Spectroscopy of ^{10}Li and ^{11}Li

M. Zinser[1], F. Humbert[2], T. Nilsson[3], W. Schwab[1], H. Simon[2], T. Aumann[4], M.J.G. Borge[5], L.V. Chulkov[6], J. Cub[1], Th.W. Elze[7], H. Emling[1], H. Geissel[1], D. Guillemaud-Mueller[8], P.G. Hansen[9], R. Holzmann[1], H. Irnich[1], B. Jonson[3], J.V. Kratz[4], R. Kulessa[10], Y. Leifels[1], H. Lenske[11], A. Magel[1], A.C. Mueller[8], G. Münzenberg[1], F. Nickel[1], G. Nyman[3], A. Richter[2], K. Riisager[12], C. Scheidenberger[1], G. Schrieder[2], K. Stelzer[7], J. Stroth[7], A. Surowiec[1], O. Tengblad[13], E. Wajda[10] and E. Zude[1]

1. Gesellschaft für Schwerionenforschung (GSI), D–64291 Darmstadt, Germany
2. Institut für Kernphysik, Technische Hochschule, D–64289 Darmstadt, Germany
3. Fysiska Institutionen, Chalmers Tekniska Högskola, S–412 96 Göteborg, Sweden
4. Institut für Kernchemie, Johannes-Gutenberg-Universität, D–55099 Mainz, Germany
5. Instituto Estructura de la Materia, CSIC, E–28006 Madrid, Spain
6. Russian Scientific Center "Kurchatov Institute", Inst. Gen. and Nucl. Phys., Moscow 123182, Russia
7. Institut für Kernphysik, Johann-Wolfgang-Goethe-Universität, D–60486 Frankfurt, Germany
8. Institut de Physique Nucléaire, BP 1, F–91406 Orsay Cedex, France
9. National Superconducting Cyclotron Laboratory and Department of Physics and Astronomy, Michigan State University, East Lansing, MI 48824, USA
10. Instytut Fizyki, Uniwersytet Jagelloński, PL–30-059 Kraków, Poland
11. Institut für Theoretische Physik, Universität Giessen, D-35391 Giessen, Germany
12. Institut for Fysik og Astronomi, Aarhus Universitet, DK–8000 Aarhus C, Denmark
13. PPE Division, CERN, CH–1211 Genève 23, Switzerland

Abstract

Break-up of secondary ^{11}Li ion beams (280 MeV/nucleon) on C and Pb targets into ^{9}Li and neutrons is studied experimentally. Cross sections and neutron multiplicity distributions are obtained, characterizing different reaction mechanisms. Invariant-mass spectroscopy for ^{11}Li and ^{10}Li is performed. The E1 strength distribution, deduced from electromagnetic excitation of ^{11}Li up to an excitation energy of 4 MeV comprises $\sim$ 8% of the Thomas-Reiche-Kuhn energy-weighted sumrule strength. Two low-lying resonance-like structures are observed for ^{10}Li at decay energies of 0.21(5) and 0.62(10) MeV, the former one carrying 26(10)% of the strength and likely to be associated with an s-wave neutron decay. A strong di-neutron correlation in ^{11}Li can be discarded. Calculations in a quasi-particle RPA approach are compared with the experimental results for ^{10}Li and ^{11}Li.

Pacs: 25.60+v, 27.20+n, 25.70.Mn, 25.70.De

Keywords: Secondary beams, halo nuclei, ^{11}Li, ^{10}Li, break-up reactions, electromagnetic excitation, invariant-mass spectra, E1-strength, nuclear resonances.

1. Introduction

After the first experiments on high-energy fragmentation of radioactive beams [1] special interest was attached to the case of ^{11}Li with its two loosely bound neutrons, which form a halo surrounding a ^{9}Li core. As discussed in several recent reviews [2], [3], [4], a number of detailed studies of nuclear and Coulomb fragmentation processes have attempted to clarify the halo's internal structure. Early hopes that the final momentum distributions would simply be those of the initial state had to give place for the realization that the initial state, the selectivity of the reaction mechanism, and the structure of the final system all have to be considered. Especially important was the realization by Barranco et al. [5] that the narrow momentum distribution of neutrons from reactions of ^{11}Li with light targets represented a final-state interaction corresponding to a low-lying virtual s- or p-state in the neutron-unbound ^{10}Li.

The problem has two facets: (i) The assumed three-body character of the ^{11}Li ground state is expected to manifest itself via mixing of the two-neutron single particle configurations based on the $p_{1/2}$ state and on the $s_{1/2}$ intruder state, the latter forming the ground state of the neighbouring ^{11}Be. Experimental evidence is now beginning to accumulate that the mixing is, indeed, appreciable. (ii) The second experimental challenge is to quantify the interactions in the n+^{9}Li system, where an essential step forward was the observation [6] of a state near the threshold. In a previous paper [7] we showed via a selection-rule argument that the neutron of this ^{10}Li virtual state almost certainly must have the same angular-momentum assignment as the ^{11}Be ground state, i.e. $1/2^{+}$.

In this paper, we present results from a study of fragmentation of ^{11}Li at 280 MeV/nucleon on C and Pb targets into the core nucleus ^{9}Li and neutrons. A kinematically complete measurement of residues of near projectile rapidity was performed, allowing for invariant-mass spectroscopy of both, the ^{11}Li and ^{10}Li nuclei. By means of this method, the E1-strength distribution of ^{11}Li and resonance (-like) structures in ^{10}Li were determined. From the measured cross sections and neutron multiplicities, details of the reaction mechanisms could be extracted. Calculations in a quasi-particle RPA (QRPA) approach were compared with the experimental data illuminating the single particle structure of the two nuclei under investigation.

2. Experimental Method

A primary beam of ^{18}O with an energy of 340 MeV/nucleon provided by the SIS accelerator facility at GSI, Darmstadt, was directed onto a Be production target of 8 g/cm^2 thickness. Typical intensities of 2×10^{10} ions per machine spill (of a few seconds duration) could be achieved for the ^{18}O beam. The emerging projectile fragments were magnetically separated in the FRagment Separator (FRS) [8] and secondary beams of 9.5 Tm ($\pm$ 1%) magnetic rigidity were selected for further transportation. Since essentially no degrader was used in the mid-plane focus of the FRS, the secondary beam was composed of ^{8}He, ^{11}Li and ^{14}Be ions with relative intensities of approximately 0.42, 0.50, and 0.08 and energies of 240, 280 and 305 MeV/nucleon, respectively. Weak admixtures of ^{6}He and tritons were also present.

The secondary beam was transported to the experimental area housing the secondary targets and detection devices. At the time of the experiment, a direct beam transport line between the FRS and the experimental area was not available (but is meanwhile installed) and thus, the Experimental Storage Ring (ESR) at GSI had to serve as a substitute beamline. After injection into the ESR, the secondary beam was extracted after one turn. Since the ESR/FRS facility is not optimized for such an operational mode, the transport efficiency turned out to be rather low (1-2 %). On the other hand, the beam quality with respect to momentum spread was improved correspondingly to a few per mille width. A typical secondary beam intensity of 50-100 ions per second at the target site was obtained, sufficient to carry out the experiment within about three days, although with moderate counting statistics.

The experimental apparatus used to study secondary beam-target interactions was already described in [9], and it is shown schematically in Fig. 1. Entering the experimental area, the beam traversed a multi-wire avalanche counter, a detector made of organic scintillator material of 0.5 mm thickness, and a multiwire drift chamber, all being position sensitive along the two dimensions perpendicular to the beam and serving for ray tracing of the incident beam ions. The scintillation counter, in addition, delivered a start signal for time measurements as well as a signal proportional to the energy loss of the beam in the detector, which in turn determined the nuclear charge of the incoming ion. Reactions to be studied took place in either a C target (thickness 1.29 g/cm^2) or a Pb target (0.30 g/cm^2); a measurement without target was also performed in order to control the background due to reactions

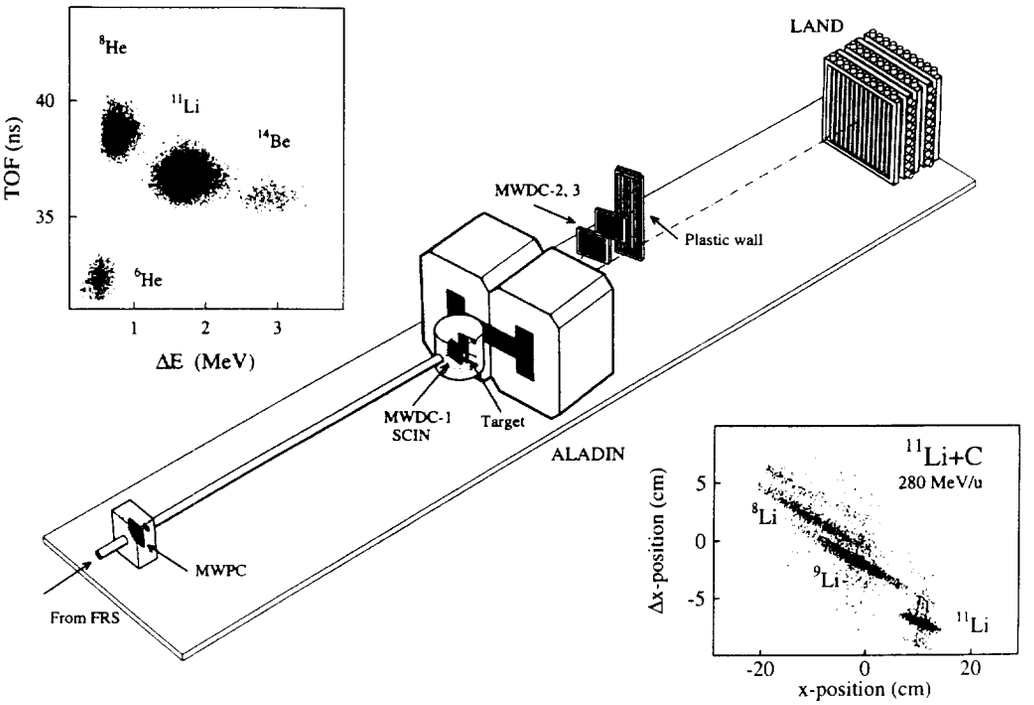

Figure 1: Schematic view of the experimental set-up, showing the scintillation detectors (SCIN, Plastic wall), multi-wire avalanche (MWPC) and multi-wire drift chambers (MWDC-1,2,3), the dipole magnet (ALADIN), the neutron detector (LAND) and target. Secondary beams are delivered by the FRS.
Inset (left hand): Identification of the incident beam ions by means of energy-loss (ΔE) and time-of-flight measurements (TOF).
Inset (right hand): Identification of the nuclear mass of fragments by means of position (x) measurements in MWDC-2 and MWDC-3 after preselection of ^{11}Li beams and Li fragments.

or beam ions, leaving the vacuum vessel right after the magnet into air. The vacuum vessel was closed by a 1 mm thick window of mixed organic compounds. Two multiwire drift chambers, separated by 1 m distance and placed right behind the magnet, served to determine the position and deflection angle of the fragment (or beam) in two dimensions. The drift chambers were operated with a mixture of Ar (65 %) and isobutane (35 %) gas at atmospheric pressure. For technical details concerning the drift chambers

and the calibration procedures we refer to [9]. An array of seven scintillation detectors (organic material, 5 mm thick) was positioned behind the last drift chamber and gave information on the fragment energy loss and time of flight, the latter in combination with the scintillation counter in front of the target.

Neutrons arising from disintegration processes of the secondary beam ions were focussed into a narrow forward cone around the initial beam direction due to the Lorentzian boost; they passed the large gap (0.48m x 1.2m) of the magnet and hit the Large Area Neutron Detector (LAND) positioned at a distance of 11 m downstream from the target; its center was placed slightly off from the beam direction (18 cm). Since the active area of LAND amounts to 2 m x 2 m, neutron scattering angles of up to about 7° were covered. The neutron detector is assembled from a total of 200 subelements filling an active volume of 2 m x 2 m x 1 m. Neutrons are converted in the iron layers into charged particles which in turn produce scintillation light in interspersed sheets of organic scintillation material. A detailed description of the LAND detector design and its performance is found in [11].

From the light output, information on the time of flight and the position of incidence of the neutrons can be derived. Charged particles can be discriminated against neutrons by means of a wall of thin organic scintillators mounted in front of LAND (not relevant here, since charged particles are deflected from LAND in the dipole magnet under most circumstances). The internal calibration of LAND with regard to relative time and position information was obtained by tracing cosmic rays through the detector. From such a measurement, we also deduced time and position resolutions. For the time resolution we found ~500 ps (FWHM), which is close to a value of about 400 ps obtained using tagged neutrons at energies of 180-660 MeV [11]. The time resolution should be compared to the total time of flight of the neutrons amounting to 55-60 ns. The position resolution along the beam direction and in one direction perpendicular to it is determined by the geometry of the submodules of the detector, i.e. ± 5 cm (full width), while for the third dimension, the cosmic ray calibration delivers a value of 7 cm (FWHM) and the measurement with tagged neutrons resulted in 5.1 cm, independent of neutron energy. The neutron detection efficiency was also determined in a separate calibration measurement [12]; at 270 MeV neutron energy we observed a value of 0.85(2). In cases where more than one neutron hit the detector, the capability of the detector to resolve such multiple hits has to be considered. For that purpose, in the past, a calibration measurement with nearly monoenergetic neutrons between 70 and 1100 MeV was performed

[12], allowing a detailed study of the neutron-induced charged particle showers in LAND. The neutrons were produced in deuteron break-up reactions. One measurement was taken at 270 MeV/nucleon, thus being close to the relevant neutron energies in the present experiment. On the basis of these data sets, the detector response is well known and can under favorable conditions be used to unfold instrumental effects or, in the more general case, to simulate a scenario supplied by theory, and thus to disentangle instrumental and physical effects.

We shall only shortly describe the main features of the algorithm which served to disentangle the neutron induced showers in LAND in case of multiple neutron hits: First it should be noticed that on the average only 1.6 submodules of LAND are fired per incident neutron (of about 280 MeV kinetic energy); this was deduce from the calibration measurement mentioned above. Starting from the submodule that was fired first, signals from submodule firing subsequently are associated to the same neutron, if (i) these subsequent hits are located in a cylindrical 'shower' volume of 29 cm radius and 50 cm depth around the first hit, or (ii), for larger distances, if they fullfil the kinematical conditions of quasi-free (n,n') scattering (the latter criterion is of less importance). For the signals from the remaining submodules the procedure is re-iterated. Heuristically, by inspecting mixed events obtained from the neutron calibration measurement, this procedure was found to provide satisfying results. For illustration, we show in Table 1 the experimentally determined multiple-hit-resolving power of LAND for a situation adjusted to that of a ^{11}Li beam (270 MeV/nucleon) impinging onto a Pb target and disintegrating with subsequent neutron emission. In this simulation, the LAND response was generated by an neutron-event-mixing procedure based on the single-neutron response observed experimentally in the calibration measurement (see above). For example, it is observed that on the average two neutrons impinging onto the detector are well recognized in 50 % of the events. We also like to point out, that even two neutrons incident with zero relative angle can be disentangled in about 10 % of such cases. This can be qualitatively understood by comparing the depth of the 'shower' volume (50 cm) with the total depth of the detector (100 cm) and taking into account the mean interaction length of about 35 cm for energetic neutrons in LAND. Therefore, a differential efficiency dependent on the neutron-neutron relative angle arises which e.g. is reflected, and to most extent determines the efficiency shown in Fig. 2 (see also section 3.2).

In Table 2 we summarize the transverse momentum acceptance and res-

Table 1: Multiple-hit-resolving power of LAND for events where one or two neutrons (270 MeV/nucleon) hit the detector simultaneously. The physical conditions were adjusted as close as possible to the circumstances of the present experiment with a ^{11}Li beam (Pb target). The numbers in the matrix give the average probability (in %) that an event with n neutrons is interpreted as an event with m neutrons.

m =	0	1	2	3
n=1	15	80	5	0
n=2	2	44	50	4

olutions for fragments and neutrons for the case of the ^{11}Li$\rightarrow^{9}$Li+xn reactions. We also include the resolutions for the measurement of the fragment and neutron velocity. The absolute calibration for the time of flight of the fragment was obtained by using beam ions in a measurement without target and by sweeping the beam across the seven modules of the plastic detector (see above); also the time resolution (FWHM=900-1300 ps) was determined in this way. For the neutron detector, a similar procedure was attempted, however, only two of the 200 detector modules could be illuminated. Therefore, the absolute time calibration was obtained using neutrons from ^{11}Li reactions in the C target, assuming that they, on the average, are of projectile velocity. In principle, one could argue that this assumption is not correct, since the ^{11}Li ions could be decelerated during the collision due to the Coulomb field as dicussed in [13] and consequently, the velocity of the break-up neutrons could be smaller than that of the projectile. We estimated, however, that because of the high bombarding energy and because of the low nuclear charge of the carbon target, such effects result in negligible shifts of the neutron time-of-flight [14]. The results from the two methods deviated only by 400 ps, which may thus be considered as a measure of the systematic error of the absolute neutron time-of-flight measurement.

Data were recorded for events which yielded a coincident trigger in the neutron and fragment detectors. In addition, down-scaled data were taken whenever a beam particle arrived at the target; this class of accepted events served to normalize the data to the beam flux, but also allowed to determine cross sections for reactions which yielded no neutron.

Table 2: Acceptance in transverse momentum $\Delta p_\perp$ for ^{9}Li fragments and neutrons and resolutions for transverse momentum $\delta p_\perp$ (FWHM) and velocity $\delta\beta$ (FWHM) with β=v/c. Average numbers are quoted, the values depend slightly on the particular reaction under consideration.

	$\Delta p_\perp$[MeV/c]	$\delta p_\perp$[MeV/c]	$\delta\beta$
Fragment	$\pm$ 300	15	0.02
Neutron	$\pm$ 60	8	0.012

3. Data Analysis and Evaluation

3.1 Data Analysis

It is the goal of the analysis to obtain the momenta of charged fragments and accompaning neutrons in order to establish neutron-fragment correlations, classified according to different types of reactions. In this paper we focus on halo-breakup reactions of the type ^{11}Li$\rightarrow^9$Li+xn (x=0,1,2). The first steps of the analysis are:

(i) identification of the incident secondary beam ion with respect to its nuclear mass and charge,

(ii) identification of the charged fragment in the same sense,

(iii) determination of the number of accompagnying neutrons,

(iv) determination of the momenta $\vec{p_F}$ of the fragment and that of coincident neutrons $\vec{p_n}$.

A beam particle is identified by its energy loss (ΔE) in the scintillation detector positioned in front of the target and by the time of flight (ToF) of the beam or the emerging fragment, measured between this detector and the second scintillation counter positioned behind the magnet (the projectile fragments essentially have the same velocity as the projectile). In Fig. 1, we present such a two-dimensional plot of ΔE vs. ToF, illustrating the procedure. Evidently, the three beam constituents of interest ^{8}He, ^{11}Li and ^{14}Be, can be identified uniquely. The beam momentum is then well defined for each species because of the stringent magnetic filtering during beam transport (see chapter 2). The nuclear charge Z_F of the fragment is obtained from

a ΔE measurement in the second scintillation counter behind the magnet (resolution δZ_F(FWHM) / Z_F $\approx$15% on the average). The nuclear mass A_F can be determined from the measurement of the magnetic rigidity of the fragment, utilizing the position information from the two drift chambers behind the magnet, projected along the direction perpendicular to the magnetic field. This procedure is illustrated in Fig. 1 for the case of fragments of Z_F = 3. The difference in magnetic rigidity between two neighboring fragment masses, after preselecting Z_F, amounts to $\sim$10 %, and thus is considerably larger than a change in rigidity due to a variation in the fragment total momentum, which is of the order of or below a few percent [15]. Thus, different masses can be separated easily. Finally, we derive both the neutron and fragment momenta from the respective position and time-of-flight measurements. Resolutions obtained for relevant quantities were already given in Table 2. Therein, effects due to beam spread and straggling in the target and detector material are incorporated, the contributions from which could be determined by inspecting events where no interaction took place in the target.

3.2 Data Evaluation

The data analysis as outlined above yields an event classification in terms of the observed fragment and its associated neutron multiplicity. For each class of events the cross section was determined by normalising the number of observed events to target thickness and measured number of incident beam particles. In a first step, the momentum distributions for fragment and neutrons can be projected for each event class. Respective results for ^{11}Li were already published in [7],[15], [16].

In this paper, we concentrate on momentum correlations between the reaction products, in particular we analyze distributions in the invariant mass of the projectile-like residues deriving the quantity

$$\mathrm{M} = \sqrt{(\sum_i P_i)^2} - \sum_i m_i^o \quad ,$$

where m_i^o and P_i denote rest masses and the 4-momenta of the reaction partners (fragment, neutron) involved, respectively.

The quantity M is invariant under Lorentz transformations and thus independent of the coordinate frame. If interpreted in the center-of-mass (CM)

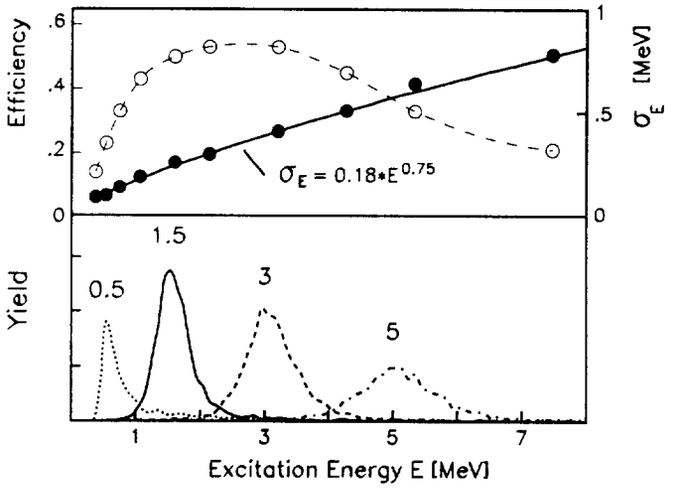

Figure 2: (Lower panel): Response of the detector system for selected excitation energies E = 0.5, 1.5, 3.0 and 5.0 MeV of ^{11}Li, disintegrating into ^{9}Li+n+n (see text).
(Upper panel): Resolution σ_E for the Gaussian part of the detector response (right hand scale, solid symbols) and detection efficiency including solid angle acceptance (lefthand scale, open symbols).

frame of the decaying system, M represents the total kinetic energy, and thus, occasionally it shall be referred to as the decay energy T_d=M. If the masses m_i^o are the disintegration products of an excited nucleus of ground state mass m_0, one obtains its excitation energy E^* simply as

$$E^* = M + \sum_i m_i^o - m_0 \quad ,$$

$\sum_i m_i^o - m_0$ obviously represents a correction for the binding energy. This is correct, if all disintegration products are in their ground states. In the most general case, the charged fragment can be excited and release its excitation energy by subsequent γ-ray emission which we do not observe. In such a case, the excitation energy E^* appears diminished by the excitation energy of the residual fragment and ambiguities can arise.

The result of such an analysis is still influenced by the response of the detector. As already discussed above, for a complex detection system in the most general case, such effects can only be studied by simulating events on the basis of an appropriate theory and by applying the experimentally determined response of the detection system. For illustration, we show in Fig. 2 results of a response simulation for the invariant mass of the ^{9}Li+n+n system for different ^{11}Li excitation energies E*. Therein we assume that the available kinetic energy is distributed among the three partners according to the available phase space. Effects due to straggling of the heavy ion in the (Pb) target, finite solid angle acceptance, detection efficiencies, resolutions for the position and time of flight for fragment and neutrons, as well as effects due to the algorithm used to disentangle the two neutron-induced showers in LAND are taken into account. The resulting distributions (Fig. 2, lower panel) exhibit a nearly Gaussian shape and a small wing towards higher excitation energies. For the Gaussian part, we observe a variance σ_{E^*} (MeV) $\approx 0.18 \cdot (E^*)^{0.75}$ with E* in MeV as shown in the upper panel of Fig. 2. The maximum detection efficiency of $\epsilon \approx 0.5$ (see Fig. 2) is obtained in the interval 1 MeV $\leq$ E* $\leq$ 4 MeV; the decrease in efficiency towards higher values of E* results from the finite solid angle acceptance for neutrons, the decrease towards lower values of E* results from the limited capability in resolving close multiple neutron hits in LAND.

4. Results and Discussion

In this chapter, we present our results for the halo-breakup reactions ^{11}Li$\rightarrow$ ^{9}Li+xn. Partly, we contrast these results with corresponding data from ^{11}Be$\rightarrow$ ^{10}Be+xn [7] and ^{8}He$\rightarrow$^{6}He+xn [9] in order to elucidate common features in halo-breakup reactions; these data were obtained in the same experiment. We first discuss cross sections and apparent neutron multiplicities and draw conclusions upon the underlying reaction mechanisms. In subsequent sections we analyze the ^{9}Li+n and ^{9}Li+n+n correlations in terms of invariant mass distributions which provide information on the intricate structure of the ^{10}Li and ^{11}Li nucleus systems.

4.1 Cross Sections, Neutron Multiplicities and Reaction Mechanisms

Table 3 summarizes the measured cross sections σ_{-2n} obtained with the

Pb and the C targets and the ^{11}Li beam. The quantity σ_{-2n} denotes the cross section for two-neutron removal from ^{11}Li. These cross sections were obtained simply by comparing the number of emerging ^{9}Li nuclei relative to that of incident ^{11}Li nuclei without any constraint. In addition, we differentiate this cross section with regard to the number of neutrons observed in LAND resulting in σ^{i}_{-2n}, where i denotes the number of neutrons. All instrumental effects, as discussed in chapters 2 and 3, are corrected for (more details can be found in [14]). We made no attempt, however, to correct for the finite solid angle coverage of the neutron-detector; the apparent neutron angular distributions, however, are dominated by a rather narrow component as we have shown in an earlier publication [7]. For this component, practically full solid angle coverage is achieved.

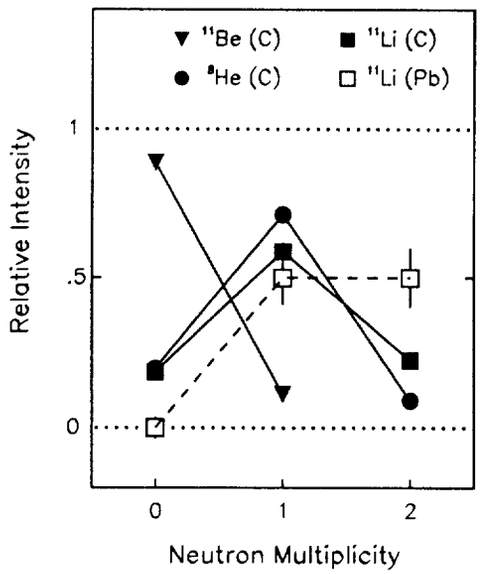

Figure 3: Neutron multiplicity distributions for breakup reactions ^{8}He (240 MeV/ nucleon)$\rightarrow^{6}$He+xn, ^{11}Li (280 MeV/nucleon)$\rightarrow^{9}$Li+xn, and ^{11}Be (460 MeV/ nucleon)$\rightarrow$ ^{10}Be+xn on targets as indicated.

From the cross sections σ^{i}_{-2n}, we can deduce the probability m_i (i = 0, 1, 2) that the halo break-up reaction is accompanied by i neutrons hitting the detector, via

$$m_i = \sigma^{i}_{-2n}/\sigma_{-2n}.$$

The mean neutron multiplicity $\bar{m} = (\sigma^{1}_{-2n} + 2\sigma^{2}_{-2n})$ / σ_{-2n} is quoted in Table 3, the multiplicity distributions are shown in Fig. 3 together with cor-

responding data for one-neutron removal reactions for ^{11}Be and two-neutron removal reactions for ^{8}He.

Commonly, three different basic reaction mechanisms are considered to be responsible for halo-breakup:

(i) electromagnetic excitation,

(ii) diffractive dissociation of one of the halo neutrons, the analogue to Fraunhofer diffractive scattering of light on a black sphere,

(iii) stripping of one of the halo neutrons by the target nucleus. This process is often referred to as 'absorption', a terminology that can be misleading, since at the high energies involved here, the struck halo nucleon will initiate an intranuclear cascade in the target with subsequent re-emission or knock-out of further nucleons. The essential feature is that, in this channel, the halo neutron will not appear in the projectile rapidity domain and escapes a detection in LAND due to large scattering angles.

The latter two processes leave a ^{9}Li+n system which is unbound and disintegrates. The ^{9}Li+n system thus acts as a 'spectator' only. The observed predominant narrow component in the neutron angular distribution is assigned to neutrons emerging from the decay of the spectator ^{10}Li. For a more detailed discussion in this spirit we refer to [17].

We first discuss the data obtained with the C target. For this case, electromagnetic excitation can be neglected: If we adopt the σ_{-2n} cross section from the Pb target as an upper limit of the electromagnetic cross section on this target and scale it according to a Z_T^2 dependence (Z_T denotes the target nuclear charge), we obtain 10 mb as an upper limit for the electromagnetic σ_{-2n} cross section with the carbon target, thus small compared to the measured cross section of 280 mb.

We then attempt to disentangle the diffractive dissociation and stripping processes on the basis of the observed neutron multiplicities. These two processes yield distinctly different neutron angular distributions and, in consequence, different neutron multiplicities: For stripping processes, re-emitted or knock-out neutrons are scattered to large angles, thus escaping a detection in LAND. We have simulated such a process using the intra-nuclear cascade

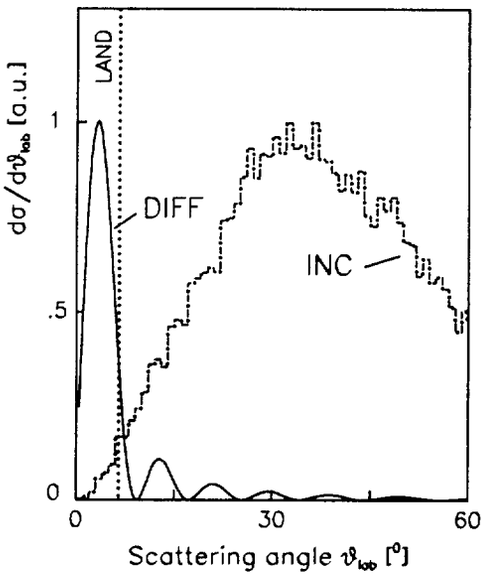

Figure 4: Cross sections $d\sigma/d\vartheta_{lab}$ in function of the laboratory scattering angle ϑ_{lab}, calculated for diffractive neutron scattering (DIFF) and for neutrons inducing an intra-nuclear cascade (INC) on a carbon target. The angular range accepted by the neutron detector (LAND) is indicated.

code Isabelle [18], treating the impinging halo neutron as a free neutron of beam velocity. The resulting angular distribution of emerging neutrons is shown in Fig. 4, where we also indicate the acceptance of LAND. Obviously, the apparent mean neutron multiplicity is practically zero for such a process. In contrast, diffractive scattering yields a forward peaked intensity profile $\sim J_1^2(\mathrm{a}p_\perp/\hbar)/p_\perp^2$ with the transverse momentum $p_\perp$, which leads to a width (FWHM) of the order $\delta p_\perp \approx \frac{3.2\hbar}{a}$ (a $= R_n + R_T$, R_n and R_T denote the radii of neutron and target) as discussed e.g. in [17](see also Fig. 4 for illustration). Consequently, the apparent neutron multiplicity $\bar{m}$ for a diffractively scattered neutron amounts to $\bar{m} = \Omega_D$, where Ω_D denotes the fraction of intensity covered by the neutron detector. In case of full solid angle coverage, i.e. $\Omega_D = 1$, the neutron multiplicity for a diffractive process would be $m^D = 1$ for a one-neutron halo nucleus (^{11}Be) and $m^D = 2$ for a two-neutron halo nucleus, while the corresponding values for stripping processes are shifted down by one unit. Inspecting the neutron multiplicity distributions shown in Fig. 3, we can already conclude that stripping processes are predominant, as the mean multiplicity for ^{11}Be is found close to zero, and for ^{11}Li and ^{8}He close to unity.

We may determine Ω_D by considering the ^{11}Be$\rightarrow^{10}$Be+n reaction on a car-

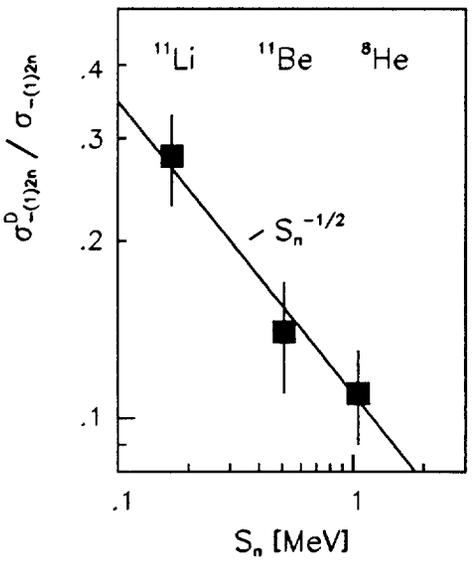

Figure 5: Contribution of the diffractive cross section σ^D_{-2n} for ^{8}He, ^{11}Li, and σ^D_{-1n} for ^{11}Be relative to the total halo break-up cross section $\sigma_{-(1)2n}$ on a carbon target versus the neutron separation energy S_n. The solid line reflects a dependence proportional to $S_n^{-1/2}$.

bon target. In this case, if a neutron is detected, it can arise from diffraction only. Our data shown in [7] led us to an estimate $\Omega_D = 0.8(0.1)$. It is straightforward to show that the diffraction cross section σ^D relative to the total halo-breakup cross section can be deduced as

$$\sigma^D_{-1n}/\sigma_{-1n} = \frac{m_1}{\Omega_D} \qquad or \qquad \sigma^D_{-2n}/\sigma_{-2n} = \frac{m_2}{\Omega_D}$$

for a one-neutron removal reaction as in ^{11}Be and for two-neutron removal as in ^{11}Li or ^{8}He, respectively.
Since diffraction is governed only by geometrical quantitities, i.e. by the radius of nucleon and target, we may adopt that Ω_D remains the same for ^{11}Be, ^{11}Li and ^{8}He reactions. We then obtain the contribution of the diffraction cross section to the halo-breakup cross section, which is shown in Fig. 5. Obviously, stripping processes are predominant. Empirically, we found a dependence of the form $\sigma^D/\sigma_{-1(2)n} \sim 1/\sqrt{S_n}$. Here, S_n denotes the neutron separation energy, for ^{11}Li and ^{8}He we adopted $S_n = \frac{1}{2}S_{2n}$. In principle, a dependence on S_n can be expected, since a minimum momentum transfer

Table 3: Measured cross section σ_{-2n} for halo-breakup of ^{11}Li (280 MeV/nucleon) on C and Pb targets. The quantities σ^{i}_{-2n} denote cross sections for reactions accompanied with i = 0,1,2 neutrons in LAND (see text). Statistical errors are quoted, systematics errors are estimated to be ~10% for the Pb target and negligible for the C target. Cross sections σ^{D}_{-2n}, σ^{S}_{-2n} and $\sigma^{e.m.}_{-2n}$ for diffractive, stripping and electromagnetic breakup as deduced in section 4.1 are also quoted. The experimentally observed mean neutron multiplicity $\bar{m}$ is given in the last line.

Target:	C	Pb
σ_{-2n} [b]	0.28 (3)	2.0 (5)
σ^{0}_{-2n} [b]	0.05 (1)	$\leq$0.07
σ^{1}_{-2n} [b]	0.17 (2)	1.0 (.35)
σ^{2}_{-2n} [b]	0.06 (2)	1.0 (.35)
σ^{D}_{-2n} [b]	0.08 (2)	
σ^{S}_{-2n} [b]	.20 (2)	
$\sigma^{e.m.}_{-2n}$ [b]	$\leq$0.01	1.5 (5)
$\bar{m}$	1.04(4)	1.5 (.15)

$\Delta p_{\perp} \approx \sqrt{2m_n S_n}$ is required in order to overcome the binding of the neutron, and thus the diffraction cross section shall be reduced with increasing binding energy.

Going from the carbon target to the lead target, we notice a drastic increase in the cross section σ_{-2n} which we naturally assign to the process of electromagnetic dissociation coming into play for heavy targets. Large cross sections with heavy targets were observed earlier in refs. [19], [20], [21], [13], [22]. In order to disentangle nuclear cross sections $\sigma^{nucl.}_{-2n}$ and electromagnetic cross sections $\sigma^{e.m.}_{-2n}$ we make use of a certain additivity in nuclear cross sections for halo nuclei, empirically observed and justified theoretically in [23]. For ^{11}Li this additivity rule reads $\sigma^{nucl.}_{-2n}$ (^{11}Li) $=\sigma_I^{nucl.}$(^{11}Li) - $\sigma_I^{nucl.}$ (^{9}Li), $\sigma_I^{nucl.}$ denoting the total nuclear interaction cross sections. Using effective sharp-cutoff radii R we can rewrite this relation into

$$\sigma^{nucl.}_{-2n}(^{11}Li) = \pi(R_{^{11}Li} - R_{^{9}Li})(R_{^{9}Li} + R_{^{11}Li} + 2R_T).$$

With $R_{^{11}Li} = 3.16$ fm [24] and $R_{^{9}Li} = 2.3$ fm [1] we obtain

$$\sigma_{-2n}^{nucl.}(^{11}Li + Pb)/\sigma_{-2n}^{nucl.}(^{11}Li + C) = 1.8 \; .$$

Subtracting the nuclear cross section $\sigma_{-2n}^{nucl.} = 0.50(5)$ b determined in this way, we get $\sigma_{-2n}^{e.m.} = 1.5(5)$ barn for ^{11}Li on a lead target.

The electromagnetic dissociation of ^{11}Li under the circumstances of the present experiment is expected to impose relatively small momentum and energy transfers. In consequence, both disintegrating neutrons should be detected in LAND. In fact, the neutron multiplicity distribution for the Pb target is shifted towards higher values in comparison to that of the C target. Subtracting the nuclear contributions as outlined above, we derive a mean neutron multiplicity $\bar{m}^{e.m.} = 1.7(2)$ for the electromagnetic halo break-up, that fits reasonably well within the expected value $\bar{m}^{e.m.} = 2$.

4.2 Neutron- and Fragment-Momentum Distributions

Momentum distributions for the ^{11}Li halo-breakup reactions were discussed already in earlier publications, both for the ^{9}Li fragment [15] and the neutrons [7]. We do not repeat the discussion presented therein, we only summarize the conclusions as far as relevant for the results given below.

From a comparison of the neutron momentum distributions from the break-up reactions ^{11}Be$\rightarrow^{9}$Li+n +X and ^{11}Li$\rightarrow^{9}$Li+n+X on a carbon target [7], together with other data quoted therein, it was deduced that the neutron momentum distribution from the ^{11}Li$\rightarrow^{9}$Li+n+x break-up can be reproduced under the assumptions

- of a diffraction component carrying about 1/3 of the neutron intensity; this could now be verified quantitatively (see section 4.1),
- of a n+^{9}Li scattering length of $\leq$ - 20 fm, leading to a virtual s-state at an excitation energy $\leq$ 50 keV in ^{10}Li,
- of a $l = 1$ resonance around an excitation energy of $\sim$ 500 keV in ^{10}Li implying $(1s_{1/2})^2$ and $(0p_{1/2})^2$ components of about equal weight in the original ^{11}Li halo ground state wave function.

Very similar conclusions were drawn recently from an analysis of the same data by Garrido et al. [25].

4.3 Invariant-Mass Spectroscopy of ^{10}Li

In this chapter, we analyse the ^{9}Li+ n momentum correlation in terms of the invariant mass M (see section 3.2).

Since M is a Lorentz-invariant quantity, it is not affected by any momentum transfer (recoil) onto the initial ^{11}Li prior to disintegration or onto the ^{10}Li subsystem, if formed during the reaction. This is in contrast to respective neutron or fragment distributions, which can be influenced by recoil effects. Interpreted in the ^{9}Li+n center-of-mass coordinate frame, the quantity M represents just the sum of the kinetic energies of ^{9}Li and the neutron, i.e. their decay energy T_d=M. The following analysis is performed under the assumption that the outgoing ^{9}Li core is in its ground state. If it would be in its excited state (2.69 MeV), the corresponding fraction of intensity would have to be shifted in energy by this amount (see section 3.2). The spectral distributions $d\sigma/dT_d$ experimentally obtained for the Pb and C targets are shown in Fig. 6. We first discuss the result for the C target.
As we outlined in section 4.1, the dominant reaction mechanism is the stripping of a single halo neutron from ^{11}Li. Since the sudden approximation is applicable at our beam energy, we expect the wave function at the instant of the collision to correspond to that of ^{11}Li, but, as discussed in the introduction, the final result will be modified strongly by final-state interactions. This effect can be calculated, as shown in our previous paper [7], by expanding the wave function of the collision complex into the eigenstates of the final system. This procedure is fairly transparent for a p-state system, which has a well-defined resonance, and, of course, also for higher angular momenta (the exact shape, however, may still depend on how the resonance was formed). For an s-state neutron, however, there is no resonance, strictly speaking, and our estimates show that the final result is very sensitive to the $(1s_{1/2})^2$ component of the initial ^{11}Li wave function. Even if we place the virtual state as high as 800 keV corresponding to an s-wave scattering length of -5 fm, we still find a strong concentration of final intensity below 0.5 MeV and peaking near 0.1 MeV. For this reason, the following analysis and also the parametrization of Table 4 should be viewed as a guide only.

The above assumptions can be verified to some extent, by inspecting corresponding data which we have obtained from the halo-breakup of ^{8}He [9]; the spectrum is shown in Fig. 7. The ^{7}He ground state is known to be

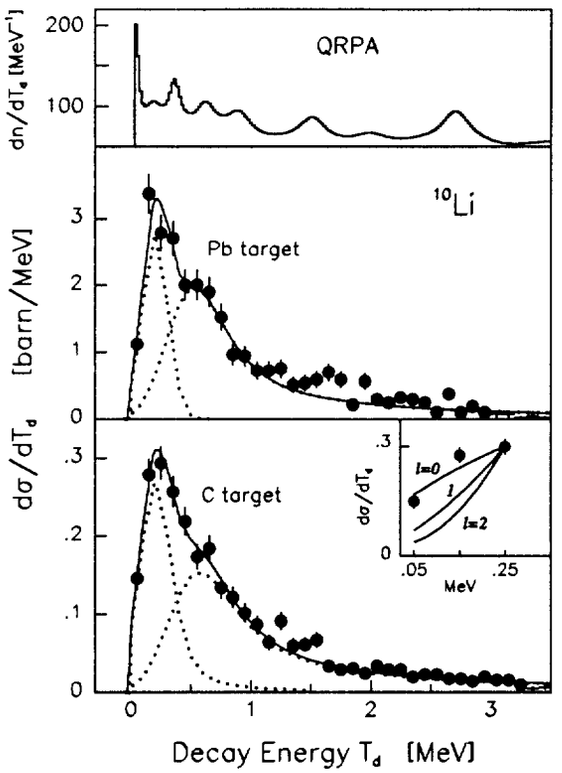

Figure 6: Decay energy (T_d) spectra for ^{10}Li obtained from an invariant-mass analysis of ^{9}Li+n after break-up of ^{11}Li in a Pb target (middle panel) and in a C target (bottom panel). The spectra are decomposed into two components (dashed lines) as discussed in the text. The inset shows the spectrum at lowest energies ($T_d \leq 250$ keV) in comparison to cross sections expected for $l = 0, 1, 2$ neutron waves (see text).
The top panel shows the ^{10}Li level density dn/dT_d obtained from the QRPA calculation.

unbound by 440(30) keV and with a width of 160(40) keV; no other resonance has been found so far for this nucleus [26]. Presumingly, the ground state configuration of ^{7}He is of neutron-$p_{3/2}$ nature. As seen from Fig. 7, the $d\sigma/dT_d$ cross section distribution can be well fitted by a Breit-Wigner function (the width of which includes a transmission coefficient for l-wave neutrons, here $l = 1$); the resulting parameters for peak energy and width are consistent with the known values [26]. Obviously, the data are rather free of (physical) background, and, at least in this case, the effects of distortions due the reaction mechanism are weak.

Returning to ^{10}Li, we first observe - in contrast to ^{7}He - a rather sudden onset of cross section at energy $T_d = 0$, already indicative of an $l = 0$ neutron wave: From general arguments it is known [27] that the neutron decay cross

section rises as $(T_d)^{l+1/2}$ with the available energy T_d and the neutron angular momentum l; thus the steepest rise is obtained for $l = 0$. The inset of Fig. 6 shows the low-energy part of the measured cross section in comparison to the $T_d^{l+1/2}$ dependence ($l = 0, 1, 2$), normalized to the maximum cross section found at $T_d = 250$ keV; the calculated cross section is folded with the experimental resolution. Apparently, the low-energy behaviour is only reproduced for $l = 0$, thus indicating a low-lying neutron $s_{1/2}$ scattering state. This would confirm our earlier conclusions summarized in section 4.2. In the case of ^{7}He we are dealing with a p-wave resonance, the low-energy behaviour is shown as well in Fig. 7 (inset). Obviously, the data are compatible with $l = 1$, while $l = 0$ can be excluded as expected.

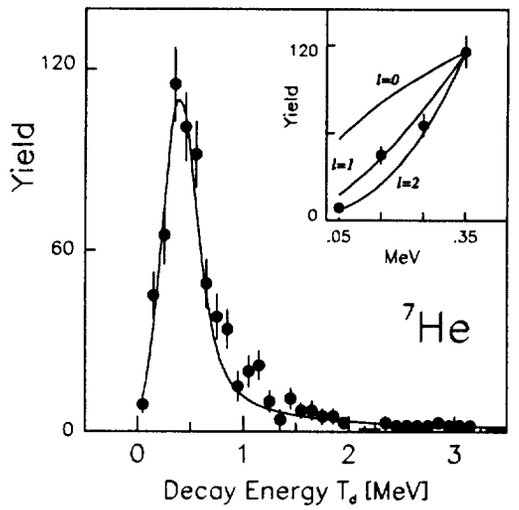

Figure 7: Decay energy (T_d) spectrum for ^{7}He obtained from an invariant-mass analysis of ^{6}He + n after break-up of ^{8}He on a C target. The solid line represents a Breit-Wigner shape using parameters quoted in [26] for peak energy and width. As in Fig. 6, the inset shows the low-energy behaviour in comparison to that expected for $l = 0, 1, 2$ neutron waves.

For ^{10}Li, a second structure is observed at higher energies. As shown in Fig. 6, we have decomposed the measured cross section into two components, for each one adopting a Breit-Wigner shape as in the case of ^{7}He. The parameters of the Breit-Wigner function fitted to the spectrum are found in Table 4. We are aware that this may not be the ideal parametrization of a virtual s state (see above) but have done so to be consistent with other papers on the subject (cf. the summary given in Table 4).

In Table 4 we include results from other measurements (see citations in Table), where resonance-like structures were observed at low energies. After

Table 4: Apparent peak energy E_o, width (FWHM) Γ_o and relative intensity I_o for resonance-like structures in ^{10}Li from this measurement (see text). Relevant results from other measurements are included. Tentative values are placed in parenthesis.

reference:	this work	[29]	[30]	[31]	[32]
E_o [MeV]	0.21(5)	0.24(6)	0.15(15)		($\geq$0.10)
Γ_o [MeV]	0.12(+.10,-.05)				($\leq$ 0.23)
I_o	0.26(10)				
E_o [MeV]	0.62(10)	0.53(6)			0.54(6)
Γ_o [MeV]	0.6(1)	0.30(8)			0.36(2)
I_o	0.74(10)				
E_o [MeV]	($\sim$1.6)	1.40(8)		0.80(25)	
Γ_o [MeV]				1.2(.3)	

some controversies in the past, now a rather consistent picture evolves for the low-energy excitations of ^{10}Li. The only truly remaining discrepancy is the fact that the lowest state is being assigned to a p-wave neutron in [28], [29], while selection-rule arguments given in our previous paper [7], and also the analysis of the low-energy behaviour given above indicate considerable contributions from s-wave neutrons. Both assignments would be compatible with the experiment of Kryger et al. [6]. It is clearly a possibility that both states contribute at low energy.

Very likely, the second component can be associated with the $l = 1$ neutron resonance which we adopted in our earlier analysis of momentum distributions. From the present analysis we find an intensity ratio of about 1:4 for the $l = 0$ to $l = 1$ components, somewhat deviating from our assumptions made in our ealier publication (see section 4.2). In addition, the spectra obtained both with the C and Pb targets (Fig. 6) exhibit also a weak indication of a broad structure centered around a decay energy of about 1.6 MeV, thus close to a peak observed in [29] (see Table 4). Considering the ^{9}Li+n spectrum obtained with the Pb target (Fig. 6), we notice that this spectrum exhibits essentially the same features as that for the C target. For the Pb target, only about 25 % of the observed cross section are due to an nuclear interaction mechanism (see section 4.1 and Table 1), while elec-

tromagnetic excitation dominates. Nevertheless, it is conceivable that after electromagnetic excitation, due to final state interaction a ^{10}Li subsystem is formed between the ^{9}Li fragment and one of the neutrons, the decay of which reflects its intrinsic properties as in the case of nuclear one-neutron stripping. Thus, since partly different reaction mechanisms are involved, we may gain further support that the observerd structures indeed reflect the nuclear response rather than arise from an intricate reaction mechanism.

Our conclusions drawn above are corroborated by results from QRPA calculations. The implications of this calculation are discussed below in a separate section.

4.4 Invariant-Mass Spectroscopy of ^{11}Li

Invariant-mass spectra could be deduced as well from the 3-body momentum correlations of the ^{9}Li+n+n system. As shown in chapter 3, the resulting spectra may also be interpreted in terms of the excitation energy E* of ^{11}Li prior to dissociation. In Fig. 8, we show the cross section distributions $d\sigma/dE^*$ from this experiment.

We focus on a discussion of the data obtained with the Pb target. As shown in section 4.1, electromagnetic excitation is predominant for the Pb target. The spectrum for the Pb target (Fig. 8) exhibits a concentration of the cross section at excitation energies below 4 MeV. Above E* = 4.1 MeV decay channels are open yielding fragments other than the ^{9}Li, which are not comprised in our data considered here. Multipole strength distributions can readily be extracted from measured electromagnetic cross sections by means of the semi-classical method [33], [34]. We first notice that the entire $d\sigma/dE^*$ distribution can be interpreted as an electric excitation of multipolarity λ = 1: For example, if we adopt a certain fraction of the energy-weighted sumrule (EWSR) strength for E1 or E2 excitations being placed at E* = 1 MeV, the resulting cross section for E1 excitation would surmount that of an E2 excitation by a factor $\simeq$500. Contributions from higher multipolarities are expected to be negligible as well. In order to extract multipole transition strength from electromagnetic heavy-ion cross sections, knowledge of the minimum impact parameter is required, below which nuclear processes become dominant. We chose the sum of the ^{11}Li and ^{208}Pb interaction radii. We notice, however, that a change of the minimum impact parameter by two fm yields a change of 10% in the E1 strength only.

Guided by the data of Fig. 8, we have tentatively decomposed the E1

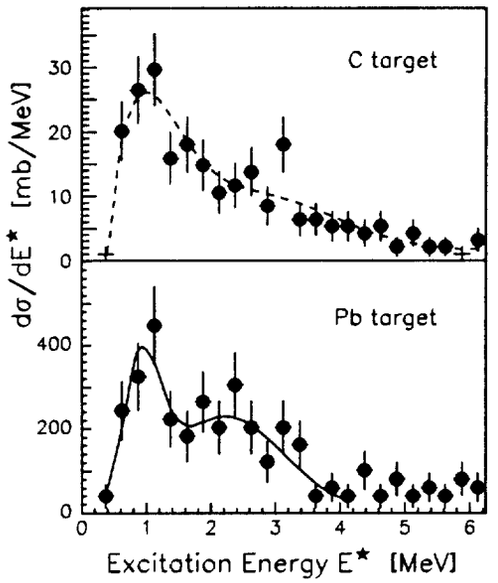

Figure 8: Excitation energy (E^*) spectra for ^{11}Li obtained from an invariant-mass analysis of ^{9}Li+n+n after break-up of ^{11}Li on a C and a Pb target. For the Pb target, the cross section is decomposed into two components (see text), the sum of which is shown as solid line.

strength distribution into two components, each one assumed to be of Gaussian shape, the parameters of which were adjusted. We like to point out that the parametrization by means of two Gaussians does not imply resonant dipole excitations, it rather comprises the continuum response, sometimes referred to as 'direct transitions into the continuum', as well.
The strength distribution parametrized in this manner served as input for a semi-classical calculation of the electromagnetic cross section following the formalism in [33]; the results were then folded with the instrumental response and compared to the data; the resulting cross section distribution is shown in Fig. 8. The corresponding E1 strength distribution is shown in Fig. 9 together with its integrated energy-weighted strength. The parameters of the strength distribution obtained from this procedure are quoted in Table 5, where we also present relevant results from other measurements for comparison. Electromagnetic excitation of ^{11}Li was also studied in refs. [13] and [22], however at considerably lower bombarding energies of 28 MeV/nucleon and 42 MeV/nucleon, respectively. Sackett et al. [13] observed a low-lying

component centered at $E^* \simeq 1.0$ MeV which obviously corresponds to the first component obtained from our data (see Table 5). Shimoura et al. [22] observe essentially the same distribution, however with a wing extending towards higher excitation energies, i.e. into the region of the second component observed in our experiment (absolute values for the E1 strength are not quoted in [22]). The lack of cross section at higher excitation energies ($E_x \geq 2$ MeV) in the data of [13] can be readily understood, since this measurements was performed at low bombarding energies and in consequence was less sensitive to the higher-lying E1-strength, because, at low bombarding energies, the flux of virtual photons decreases rapidly towards higher frequencies.

In summary, we find an appreciable E1 strength already at low excitation energies, far out of the domain of the normal giant dipole resonance. It can be decomposed into at least two structures, both together carrying about 8% of the Thomas-Reiche-Kuhn (TRK) energy-weighted dipole sumrule strength (EWSR).

A number of theoretical attempts based on self-consistent microscopical approaches [35], [36], [37] and three-body models [38], [39] were made to predict the dipole response of ^{11}Li. Although differing in details, the various calculations bear common features: A fraction of the dipole strength is redistributed towards very low excitation energies, reflecting the dipole response of the loosely bound valence neutrons, i.e. essentially $p_{1/2}$ excitations into the s- and d-wave continuum. By comparing calculations with and without an effective ph-interaction, it is found that the low-lying strength basically represents the free valence neutron response and coherent effects forming a 'soft' dipole mode seem to be absent. More quantitatively, the calculations of [35] and [36] deliver a value of about 2% of the TRK-EWSR, if integrated in the energy interval up to 4 MeV. Thus, our experimental result of 8% is underestimated considerably.

In order to explore this discrepancy, we compare the results with QRPA calculations which we discuss in the following section.

Almost quantitative agreement is obtained from a calculation of the dipole strength in a cluster-orbital shell model [39]: Therein, two components centered at 0.7 and 2.7 MeV carrying 1% and 7% of strength, respectively, were obtained, in nearly perfect agreement with our data. The first structure was assigned to the relative motion of the halo neutrons against core, while the second structure corresponds to the core excitation of ^{9}Li into its particle-

Table 5: Components of the E1 strength distribution in ^{11}Li as obtained from this measurement. Peak energies E_o, width (FWHM) Γ_o and percentage I_o of the EWSR strength are quoted. Relevant results from other measurements are included [13], [22]. The data from refs. [41], [42], [43] represent excited state of ^{11}Li obtained with different techniques.

reference:	this work	[13]	[22]	[41]	[42]	[43]
E_o [MeV]	1.0(1)	1.0	1.0		1.25(13)	1.2(1)
Γ_o [MeV]	0.7(2)	0.8				
I_o [%]	1.2(3)	~2.				
E_o [MeV]	2.4 (2)			2.47(7)	3.0(2)	
Γ_o [MeV]	2.1(6)					
I_o [%]	7(2)					

stable excited state at 2.67 MeV. It should be noticed, that these calculations yield almost pure $p_{1/2}$ excitations. In contrast, in [38] a three-body model with a pure $(s_{1/2})^2$ ground state configuration was used, the result seems to be in fair agreement with the data, at least the lower component around 1 MeV excitation energy is reproduced.

In Table 5, we indicate also excited states, observed by other techniques than electromagnetic excitation [43], [41], [42]. Apparently, the two structures deduced here find correspondent structures in other measurements. The possible spin assigments $1/2^+$, $3/2^+$, or $5/2^+$ for the E* = 1.2 MeV state in [43] is in agreement with the fact that it can be reached via an E1 excitation. Likewise, the state at 1.25 MeV observed in inelastic proton scattering [42] exhibits an angular distribution indicating an orbital angular momentum transfer $\Delta l = 1$ [44].

4.5 Comparison of Experimental Results and QRPA Calculations

In this section, we compare the experimental results with a recent quasiparticle RPA (QRPA) calculation [40] for ^{10}Li and ^{11}Li. Preliminary QRPA results were already discussed in [37],[29], but the present calculations are refined in several aspects. A proton–neutron QRPA description for the states in ^{10}Li and a pairing approach for the ground state of ^{11}Li was used. Excited states of ^{11}Li were described by normal QRPA, i.e. a superposition of neu-

tron and proton two-quasiparticle states. In contrast, the ^{10}Li configurations are given by mixed proton-neutron two quasiparticle states.

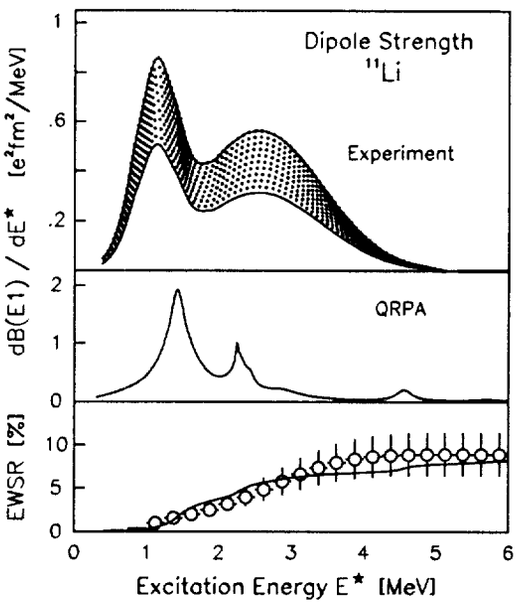

Figure 9: (top): E1-strength distribution dB(E1)/dE* (hatched area) in function of the excitation energy E* in ^{11}Li as deduced from the experiment.
(middle): same, however, as obtained from the QRPA calculation.
(bottom): energy-weighted E1 strength, integrated up to excitation energy E* and normalized to the total E1 strength. Experimental values are normalized to the TRK sum rule and are denoted by symbols. The solid curve represents the result of the QRPA calculation, the strength integrated up to 35 MeV excitation energy served for normalization.

For ^{11}Li, the QRPA calculation reveals a considerably fraction of dipole strength at low excitation energies (see Fig. 9), i.e. far below the domain of the usual giant dipole resonance. The experimental EWSR fraction, integrated up to 4 MeV excitation energy, was reproduced by lowering the initial pairing strength by 12%. With this choice, we obtain an occupation probability of close to 10% for the $1s_{1/2}$ single particle level. This result may be compared to a recent relativistic Hartree-Bogoliubov calculation [45], where an occupation probability of about 25% for the $1s_{1/2}$ level was obtained. This large difference by a factor of 2 - 3 reflects the present uncertainty in the structure of the pairing interaction. Also, it should be noticed, than an occupation probability around 50% was deduced in [7] (see previous sections) and as well from recent β-decay studies [46].

The differential E1–response function shown in Fig. 9, exhibits peak structures around 1.4 and 2.3 MeV excitation energy, thus in close corre-

spondence to the experimental data. An analysis of the QRPA calculation reveals that the lower-lying structure reflects almost pure $s_{1/2}$ excitations into the p-wave continuum with small contributions from $p_{1/2}$ excitations. To a large extent the first peak reflects the $\frac{1}{2}^-$ resonance which theoretically is also found in the ^{10}Li=^{9}Li+n system (see below). The strength around 2.3 MeV is of a more complicated structure. There, with increasing energy, the characteristic of $s_{1/2}$-excitations into the tails of the $\frac{1}{2}^-$ resonance and the non-resonant $\frac{3}{2}^-$ continuum changes rapidly to p–state excitations.

The unbound nature and the odd–odd structure of ^{10}Li pose additional problems to a theoretical description. The identification of a "ground state" is clearly hard to achieve. A reasonable choice is to look for resonances in the ^{9}Li+n scattering system. The mean–field calculation predicts a sharp $\frac{1}{2}^-$ resonance at $\epsilon = 324$ keV, but there is also s-wave strength which actually continues to increase until a maximum right at the threshold. However, the small width of the $\frac{1}{2}^-$ resonance provides very reasonable arguments to consider this as the "ground state" of ^{10}Li. The s-wave structure reflects the finite (and negative) scattering length of the n+^{9}Li mean–field but will not lead to a stable configuration, even though this indicates the existence of a virtual state.

In Fig. 6, QRPA results for the density of states in ^{10}Li are shown. The calculations include contributions from $J = 1^\pm$ to $4^\pm$ corresponding to the population of s–,p– and d–wave neutron continuum states. Right at the threshold, $J = 1^-, 2^-$ states are found where the neutron is occupying the s-wave continuum. The next structures originate from the $\frac{1}{2}^-$ resonance. The residual interations lead to a splitting of the resonance into several components. This region is dominated by $J = 1^+, 2^+$ configurations. Around 1.5 MeV a cluster of 2^- states is found which results from interfering contributions from the s-wave continuum and the low-energy tail of a $\frac{5}{2}^+$ resonance at about 4.5 MeV. The same structure is responsible for the strong component around 2.6 MeV where an equal amount of $J = 2^-, 3^-$ states appears.

It should be noticed that the level densities do not allow conclusions on the excitation probabilities of the states in a nuclear reaction. For such an analysis a quantitative dynamical description of the reaction process must be added which is not available at present. Nevertheless, as seen in Fig. 6, a number of structures in the QRPA level density may be associated with corresponding structures observed experimentally in the one-neutron strip-

ping cross section (see the discussion in section 4.3): The narrow structure at zero energy reflecting the s-wave decay, is likely to be associated with the first component resulting from our analysis of the stripping cross section (see table 3). A second group of peaks found at energies 0.3 - 0.7 MeV coincides in excitation energy with the second component deduced from the stripping cross section, although experimentally not resolved. Even an indication on the lower one of the two structures seen in the level density at energies around 1.5 and 2.6 MeV, was obtained experimentally.
In summary, it appears that the results of the QRPA calculations corroborate to most extent our phenomenological analysis performed in the previous sections, although, questions such as the $1s_{1/2}$ occupation probabilty certainly require further theoretical and experimental work.

4.6 Neutron-Neutron Correlation in ^{11}Li

It is a long standing question whether the two ^{11}Li valence neutrons are subject to strong correlations and - in the extreme case - form a dineutron cluster. We may have a rather direct approach by inspecting the momentum correlation of the two neutrons emerging after electromagnetic excitation in the Pb target. For that purpose, we have analysed the neutron-neutron (nn) invariant-mass spectrum. If interpreted in the neutron-neutron center-of-mass frame, the neutron-neutron invariant mass M_{nn} coincides with the two-neutron kinetic energy $T_{nn} = M_{nn}$.

We explore two extreme models,

- the 'phase space' model, where the available energy is partitioned among ^{9}Li and the two neutrons according to the available phase space,
- the 'dineutron' model, where both neutrons emerge with zero relative momentum, i.e. $T_{nn} = 0$.

The technical procedure is as follows: we start from the excitation energy distribution of ^{11}Li according to the experimentally determined distribution (see previous section). This excitation energy, diminished by the binding energy, is partitioned among the three constituents according to the above models, and a transformation of the resulting momenta into the laboratory frame is performed. A detector response simulation for the two neutrons follows (see chapter 2 and 3), which takes into account all instrumental effects,

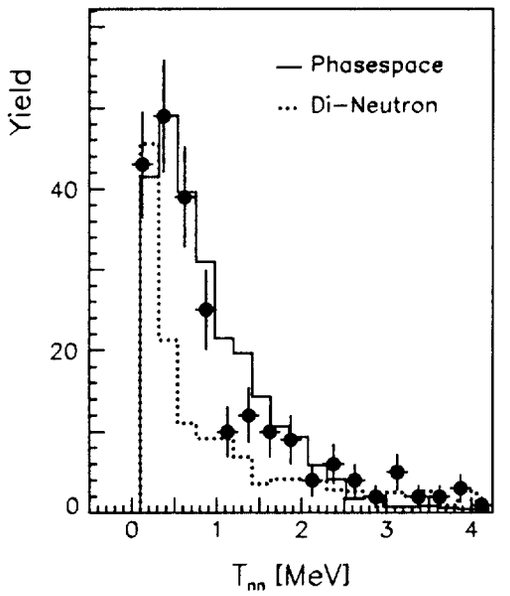

Figure 10: Neutron-neutron relative energy (T_{nn}) spectrum obtained from an invariant-mass analysis of the data from break-up of ^{11}Li on a Pb target. The curves represent the results from event simulations adopting 'phase space' and 'di-neutron' models as explained in the text.

and the resulting data are analyzed in terms of neutron-neutron invariant mass spectra in the same manner as the experimental data. In Fig. 10, we compare the measured T_{nn} distribution with the results from the two models adopted above; the calculated distributions were arbitrarily normalized to the data. Obviously, independent of the choice of normalization, the extreme di-neutron model fails in reproducing the data, while the phase space model may provide satisfying agreement.

Similar conclusions have been drawn in [47] where an isotropic distributions in the neutron-neutron relative angle in the ^{11}Li rest frame was observed and thus the di-neutron model could be discarded. Nevertheless, we cannot exclude that correlations of other type than that of extreme dineutron models exist. We also cannot ignore the fact that neutron-neutron correlations pre-existing in the ^{11}Li ground state may become distorted due to momentum transfer during the excitation process or due to final state interactions among the outgoing disintegration residues. We feel, however, that a detailed analysis of such effects would require a significantly improved statistical accuracy than available with the present data.

Summary

Halo-breakup reactions of secondary, energetic ^{11}Li ion beams interacting with a light and a heavy target were studied. From measured cross sections and neutron multiplicities, we found that stripping of one of the halo neutrons in the case of the light target, and electromagnetic dipole excitation in the case of the heavy target are the predominant reaction mechanisms. Invariant mass spectroscopy was performed for ^{9}Li+n (^{10}Li) and ^{9}Li+n+n (^{11}Li) decay systems. In the former case, two low-lying structures of comparable intensity were observed in the decay energy spectrum, the one lowest in decay energy likely reflects an s-wave decay, a result which is supported by the QRPA calculations. In the latter case, the E1 strength distribution could be mapped up to about 4 MeV excitation energy. In this region of excitation energies, an appreciable fraction of the EWSR strength, i.e. 8%, was found. As a result of the QRPA calculations we obtain that this low-lying strength basically reflects the dipole response of the halo neutrons occupying the $1s_{1/2}$ and $0p_{1/2}$ single particle orbits. In addition, on the basis of the neutron-neutron invariant mass spectrum we could exclude strong correlations between the two halo neutrons of ^{11}Li.

More generally, we believe that exclusive measurements as performed here and invariant-mass spectroscopy in particular, using energetic secondary beams, are well suited tools in exploring the structure of nuclei at and even beyond the driplines. The experimental methods are applicable even at very low secondary beam intensities, i.e. under circumstances met in experiments exploring the structure of nuclei far off stability. Invariant-mass spectroscopy allows to extract strength distributions, which appear rather undistorted and essentially free of (physical) background. Yet, a complete reaction theory, in particular for a quantitative description of stripping reactions at high bombarding energies, is still to be developed. Improvements in intensity of the secondary beams are certainly required in order to give access to more detailed investigations and to provide a better statistical significance.

The authors are indebted to the staff personel of the GSI accelerator group and of the target laboratory for their support.
We acknowledge support by the German Federal Minister for Research and Technology (BMBF) under Contracts 06DA 665 I, 06OF 112 and 06MZ 465, by GSI under Contracts DA RIK, OF ELZ, MZ KRK, by the Polish Committee of Scientific Research under Contract PBZ/PB03/113/09, EC under contract ERBCHGE-CT92-0003 and by the Spanish CICYT under contract AEN92-0788-C02-02 (MJGB).

References

[1] I. Tanihata, H. Hamagaki, O. Hashimoto, Y. Shida, N. Yoshikawa, K. Sugimoto, O. Yamakawa, T. Kobayashi and N. Takahashi, *Phys. Rev. Lett.* **55**, 2676 (1985)

[2] K. Riisager, *Rev.Mod.Phys.* **66**, 1105 (1994)

[3] P.G. Hansen, A.S. Jensen and B. Jonson, *Annu. Rev. Nucl. Part. Sci.* **45**, 591 (1995)

[4] I. Tanihata, *Prog.Part.Nucl.Phys.* **35**, 505 (1995)

[5] F. Barranco, E. Vigezzi and R. Broglia, *Phys. Lett.* **B319**, 387 (1993)

[6] R.A. Kryger, A. Azhari, A. Galonsky, J.H. Kelley, R. Pfaff, E. Ramakrishnan, D. Sackett, B.M. Sherill, M. Thoenessen, J.A. Winger and S. Yokoyama, *Phys. Rev.* **C47**, R2439 (1993)

[7] M. Zinser, F. Humbert, T. Nilsson, W. Schwab, Th. Blaich, M.J.G. Borge, L.V. Chulkov, H. Eickhoff, Th.W. Elze, H. Emling, B. Franzke, H. Freiesleben, H. Geissel, K. Grimm, D. Guillemaud-Mueller, P.G. Hansen, R. Holzmann, H. Irnich, B. Jonson, J.G. Keller, O. Klepper, H. Klingler, J.V. Kratz, R. Kulessa, D. Lambrecht, Y. Leifels, A. Magel, M. Mohar, A.C. Mueller, G. Münzenberg, F. Nickel, G. Nyman, A. Richter, K. Riisager, C. Scheidenberger, G. Schrieder, B.M. Sherrill, H. Simon, K. Stelzer, J. Stroth, O. Tengblad, W. Trautmann, E. Wajda and E. Zude, *Phys. Rev. Lett.* **75**, 1719 (1995)

[8] H. Geissel, P. Armbruster, K. Behr, A. Brünle, K. Burkard, M. Chen, H. Folger, B. Franczak, H. Keller, O. Klepper, B. Langenbeck, F. Nickel, E. Pfeng, M. Pfützner, E. Roeckl, K. Rykaczewski, I. Schall, D. Schardt, C. Scheidenberger, K.-H. Schmidt, A. Schröter, T. Schwab, K. Sümmerer, M. Weber, G. Münzenberg, T. Brohm, H.-G. Clerc, M. Fauerbach, J.-J. Gaimard, A. Grewe, E. Hanelt, B. Knödler, M. Steiner, B. Voss, J. Weckenmann, C. Ziegler, A. Magel, H. Wollnik, J. Dufour, Y. Fujita, D. Viera and B. Sherrill, *Nucl. Instr. and Meth. in Phys. Research* **B70**, 286 (1992)

[9] T. Nilsson, F. Humbert, W. Schwab, H. Simon, M.H. Smedberg, M. Zinser, Th. Blaich, M.J.G. Borge, L.V. Chulkov, Th.W. Elze, H. Emling,

H. Geissel, K. Grimm, D. Guillemaud-Mueller, P.G. Hansen, R. Holzmann, H. Irnich, B. Jonson, J.G. Keller, H. Klingler, A.A. Korsheninnikov, J.V. Kratz, R. Kulessa, D. Lambrecht, Y. Leifels, A. Magel, M. Mohar, A.C. Mueller, G. Münzenberg, F. Nickel, G. Nyman, A. Richter, K. Riisager, C. Scheidenberger, G. Schrieder, B.M. Sherrill, K. Stelzer, J. Stroth, O. Tengblad, W. Trautmann,E. Wajda, M.V. Zhukov and E. Zude, *Nucl. Phys.* **A598**, 418 (1996)

[10] The ALADIN Collaboration, GSI Scientific Report, Darmstadt, 292 (1989)

[11] T. Blaich, T. W. Elze, H. Emling, H. Freiesleben, K. Grimm, W. Henning, R. Holzmann, G. Ickert, J. G. Keller, H. Klingler, W. Kneissl, R. König, R. Kulessa, J. V. Kratz, D. Lambrecht, J. S. Lange, Y. Leifels, E. Lubkiewicz, M. Proft, W. Prokopowicz, C. Schütter, R. Schmidt, H. Spies, K. Stelzer, J. Stroth, W. Walus, E. Wajda, H. J. Wollersheim, M. Zinser and E. Zude (LAND Collaboration), *Nucl. Instr. and Meth. in Phys. Research* **A314**, 136 (1992)

[12] LAND Collaboration, GSI Scientific Report, Darmstadt, 275 (1994)

[13] D. Sackett, K. Ieki, A. Galonsky, C. Bertulani, H. Esbensen, J. Kruse, W. Lynch, D. Morrissey, B. Sherrill, H. Schulz, A. Sustich, J. Winger, F. Deák, Á. Horváth, Á. Kiss, Z. Seres, J.J. Kolata, R.E. Warner and D.L. Humphrey, *Phys. Rev.* **C48**, 118 (1993)

[14] M. Zinser, thesis, Johannes Gutenberg-Universität Mainz, Mainz (1996)

[15] F. Humbert, T. Nilsson, W. Schwab, M.Zinser, T. Blaich, M. Borge, L. Chulkov, H. Eickhoff, T. Elze, H. Emling, B. Franzke, H. Freiesleben, H. Geissel, K. Grimm, D. Guillemaud-Mueller, P.G. Hansen, R. Holzmann, H. Irnich, L. Johannsen, B. Jonson, J. Keller, O. Klepper, H. Klingler, J.V. Kratz, R. Kulessa, D. Lambrecht, Y. Leifels, A. Magel, M. Mohar, A. Mueller, G. Münzenberg, P. Møller, F. Nickel, G. Nyman, A. Richter, K. Riisager, C. Scheidenberger, G. Schrieder, B. Sherrill, H. Simon, K. Stelzer, J. Stroth, O. Tengblad, W. Trautmann, E. Wajda and E. Zude, Phys. Lett. **B347**, 198 (1995)

[16] T. Nilsson, Th. Blaich, M.J.G. Borge, L.V. Chulkov, Th.W. Elze, H. Emling, H. Geissel, K. Grimm, D. Guillemaud-Mueller, P.G. Hansen,

R. Holzmann, P. Hornshøj, F. Humbert, H. Irnich, L. Johannsen, B. Jonson, M. Keim, J.G. Keller, H. Klingler, J.V. Kratz, R. Kulessa, D. Lambrecht, Y. Leifels, M. Lewitowicz, A. Magel, M. Mohar, A.C. Mueller, G. Münzenberg, R. Neugart, F. Nickel, G. Nyman, A. Richter, K. Riisager, M.-G. Saint-Laurent, C. Scheidenberger, G. Schrieder, W. Schwab, B. Sherrill, H. Simon, O. Sorlin, K. Stelzer, J. Stroth, O. Tengblad, E. Wajda, K. Wilhelmsen Rolander, M. Zinser and E. Zude, *Europhys. Lett.* **30**, 19 (1995)

[17] F. Barranco, E. Vigezzi and R.A. Broglia, *Z. Phys.* **A356**, 45 (1996)

[18] Y. Yariv and Z. Fraenkel, *Phys. Rev.* **C20**, 2227 (1979)

[19] T. Kobayashi, S. Shimoura, I. Tanihata, K. Katori, K. Matsuta, T. Minamisono, K. Sugimoto, W. Müller, D. Olson, T. Symons and H. Wieman, *Phys. Lett.* **B232**, 51 (1989)

[20] K. Riisager, R. Anne, S. Arnell, R. Bimbot, H. Emling, D. Guillemaud-Mueller, P. Hansen, L. Johansen, B. Jonson, A. Latimier, M. Lewitowicz, S. Mattson, A. Mueller, R. Neugart, G. Nyman, F. Poughenon, A. Richard, A. Richter, M. Saint-Laurent, G. Schrieder, O. Sorlin and K. Wilhelmsen, *Nucl. Phys.* **A540**, 365 (1992)

[21] B. Blank, J.-J. Gaimard, H. Geissel, K.-H. Schmidt, H. Stelzer, K. Sümmerer, D. Bazin, R. Del Moral, J.P. Dufour, A. Fleury, F. Hubert, H.-G. Clerc and M. Steiner, *Nucl. Phys.* **A555**, 408 (1993)

[22] S. Shimoura, T. Nakamoura, M. Ishihara, N. Inabe, T. Kobayashi, T. Kubo, R.H. Siemssen, I. Tanihata and Y. Watanabe, *Phys. Lett.* **B348**, 29 (1995)

[23] Y. Ogawa, K. Yabana and Y. Suzuki, *Nucl. Phys.* **A543**, 722 (1992)

[24] I. Tanihata, T. Kobayashi, O. Yamakaw, S. Shimoura, K. Ekuni, H. Sugimoto, N. Takahashi, T. Shimoda and H. Sato, *Phys. Lett.* **B206**, 592 (1988)

[25] E. Garrido, D.V. Fedorov and A.S. Jensen, *Phys.Rev.* **C53**, 3159 (1996), and preprint, Aarhus University, Aarhus (1996)

[26] F. Ajzenberg-Selove, *Nucl. Phys* **A490**, 1 (1988)

[27] J.M. Blatt and V.F. Weisskopf, Theoretical Nuclear Physics, Springer Verlag, New York Heidelberg Berlin, chapt. 8 (1979)

[28] H.G. Bohlen, B. Gebauer, M. von Lucke-Petsch, W. von Oertzen, A.N. Ostrowski, M. Wilpert, Th. Wilpert, H. Lenske, D.V. Alexandrov, A.S. Demyanova, E. Nikolskii, A.A. Korsheninnikov, A.A. Ogloblin, R. Kalpakchieva, Y.E. Penionzhkevich and S. Piskor, *Z. Phys.* **A344**, 381 (1993)

[29] H.G. Bohlen, W. von Oertzen, Th. Stolla, R. Kalpakchieva, B. Gebauer, M. Wilpert, Th. Wilpert, A.N. Ostrowski,S.M. Grimes and T.N. Massey, Proc. IV Int. Conf. on Radioactive Nuclear Beams, Omiya, Japan (1996), *Nucl. Phys.* **A**, in press

[30] A.I. Amelin, M.G. Gornov, Yu.B. Gurov, A.L. II"in. P.V. Morokhov, V.A. Pechkurov, V.I. Savel'ev, F.M. Sergeev, S.A. Smirnov, B.A. Chernyshev, R.R. Shafigulin and A.V. Shiskov, *Sov. J. Nucl. Phys.* **52**, 782 (1990)

[31] K.H. Wilcox, R.B Weisenmiller, G.J. Wozniak, N.A. Jelley, D. Ashery and J. Cerny, *Phys. Lett.* **B59**, 142 (1975)

[32] B.M. Young, W. Benenson, J.H. Kelley, N.A. Orr, R. Pfaff, B.M. Sherrill, M. Steiner, M. Thoennessen, J.S. Winfield, J.A. Winger, S.J. Yennello and A. Zeller, *Phys. Rev.* **C49**, 279 (1994)

[33] A. Winther and K. Alder, *Nucl. Phys.* **A319**, 518 (1979)

[34] C. A. Bertulani and G. Baur, *Phys. Reports* **163**, 299 (1988)

[35] G. Bertsch and J. Foxwell, *Phys. Rev.* **C41**, 1300 (1990); ibid, **C42**, 1159 (1990)

[36] S.A. Fayans, *Phys. Lett.* **B267**, 443 (1991)

[37] H. Lenske, Proc. Int. Symposium on Structure and reactions of unstable Beams, Niigata, Japan, World Scientific, Singapore New Jersey London Hong Kong, p.194 (1991)

[38] B. Danilin, I.J. Thompson, M.V. Zhukov, J.S. Vaagen and J.M. Bang, *Phys. Lett.* **B333**, 94 (1994)

[39] Y. Suzuki and Y. Tosaka, *Nucl. Phys.* **A517**, 599 (1990)

[40] H. Lenske, to be published

[41] H.G. Bohlen, R. Kalpakchieva, D.V. Aleksandrov, B. Gebauer, S.M. Grimes, T. Kirchner, M. von Lucke-Petsch, T.N. Massey, I.G. Mukha, W. von Oertzen, A.A. Ogloblin, A.N. Ostrowski, C. Seyfert, T. Stolla, M. Wilpert and Th. Wilpert, *Z. Phys.* **A351**, 7 (1995)

[42] A.A. Korsheninnikov, E.Yu Nikolskii, T. Kobayashi, A. Ozawa, S. Fukuda, E.A. Kuzmin, S. Momota, B.G. Novatskii, A.A Ogloblin, V. Pribora, I. Tanihata, and K. Yoshida, Phys. Rev. **C55**, R537 (1996)

[43] T. Kobayashi, *Nucl. Phys.* **A538**, 343c (1992)

[44] A.A. Korsheninnikov, Proc. IV Int. Conf. on Radioactive Nuclear Beams, Omiya, Japan (1996), *Nucl. Phys.* **A**, in press

[45] J. Meng and P. Ring, *Phys. Rev. Lett.* **77**, 3963 (1996)

[46] M.J.G. Borge, H. Fynbo,D. Guillemaud-Mueller, P. Horsnhoj, F. Humbert, B. Jonson, T.E. Leth, G. Martinez-Pinedo, T. Nilsson, G. Nyman, A. Poves, I. Ramos-Lerate, K. Riisager, G. Schrieder, M. Smedberg, O. Tengblad and the Isolde collaboration, *Phys. Rev. Lett.*, January 1997, and to be publ. in *Nucl. Phys.*

[47] K. Ieki, A. Galonsky, D. Sackett, J. Kruse, W. Lynch, D. Morrissey, N. Orr, B. Sherrill, J. Winger, F. Deák, Á. Horváth, Á. Kiss, Z. Seres, J.J. Kolata, R.E. Warner and D.L. Humphrey, preprint, Michigan State University, Michigan (1996)